Nano Energy (2015) 13, 537–545

Available online at www.sciencedirect.com

ScienceDirect

journal homepage: www.elsevier.com/locate/nanoenergy

RAPID COMMUNICATION

Roll-to-roll fabrication of organic nanorod electrodes for sodium ion batteries

Chao Luo[a], Jingjing Wang[b], Xiulin Fan[a], Yujie Zhu[a], Fudong Han[a], Liumin Suo[a], Chunsheng Wang[a,*]

[a]*Department of Chemical and Biomolecular Engineering, University of Maryland, College Park, MD 20742, USA*
[b]*Department of Chemistry and Biochemistry, University of Maryland, College Park, MD 20742, USA*

Received 22 February 2015; received in revised form 23 March 2015; accepted 29 March 2015
Available online 7 April 2015

KEYWORDS
Organic electrode;
Na-ion batteries;
Anode;
Nanorod;
Roll-to-roll fabrication

Abstract
Organic electroactive materials derived from biomasses are promising candidates for next generation rechargeable batteries due to the low cost, sustainability and environmental benignity. Since organic materials have very low electronic conductivity, they are normally synthesized into nano-scale and mixed with conductive carbon before electrode fabrication. Herein, we first reported a unique role-to-role fabrication technology by taking advantage of the high solubility of organic materials in water. The synthetic process of nano-size organic materials is merged into the organic electrode fabrication process. 2,5-Dihydroxy-1,4-benzoquinone disodium salt (DHBQDS) is used as a model, and the DHBQDS nanorod electrode is *in situ* formed by precipitating DHBQDS nanorods from DHBQDS–sodium alginate–carbon black aqueous slurry film on a Cu current collector during electrode drying process. Due to the fast ionic and electronic conductivity of DHBQDS–carbon nanocomposite, the DHBQDS nanorod electrodes deliver a reversible capacity of 167 mA h g^{-1} at a high current density of 200 mA g^{-1} after 300 cycles, which is 87% of its initial capacity (capacity decay rate of 0.051% per cycle). To reduce the dissolution of DHBQDS in the electrolyte upon cycling, a thin layer of Al_2O_3 with thickness of 1 nm or 2 nm is coated on the DHBQDS nanorod electrodes using atomic layer deposition (ALD). The Al_2O_3 coating remarkably suppresses the dissolution of DHBQDS nanorods as evidenced by the increased Coulombic efficiency from 94% to ~100% at a low current density of 50 mA g^{-1}. The reversible capacity of Al_2O_3 coated DHBQDS nanorod electrodes remains at 212 mA h g^{-1} after 300 cycles with a very low capacity decay rate of 0.049% per cycle. The ALD enhanced organic nanorods exhibit the best reversible capacity and cycle life among the organic electrodes reported for Na-ion batteries.

*Corresponding author.
E-mail address: cswang@umd.edu (C. Wang).

http://dx.doi.org/10.1016/j.nanoen.2015.03.041
2211-2855/

Introduction

Li-ion batteries (LIB) are the promising energy storage devices for emerging electric vehicles and smart grids. However, the high cost and limited availability of lithium sources hinder the large-scale application of LIB for renewable energy storage [1-3]. Na-ion batteries (NIB), which share similar chemistry as LIB, are the most promising energy storage devices for renewable energy due to the low cost and abundance of sodium sources [4]. Recently, considerable research efforts have been devoted to developing advanced cathode materials for NIB [5]. Among them, sulfur [6,7], selenium [8,9], O3-type and P2-type sodium metal oxides [10-12], sodium metal phosphate [13,14] and sodium metal sulfate [15] cathodes showed excellent electrochemical performance. However, there are only a few reports on the anode materials. Although the nongraphitic carbonaceous materials [16,17], tin [18,19], antimony [20], red phosphorous [21,22] and metal sulfides [23,24] anodes show promising performance in NIB, the high energy-consuming synthetic process, material scarcity, and high cost limit the wide application of these anode materials in NIB. As a consequence, it is of great significance to explore energy- and cost-effective organic anode materials for NIB.

Organic materials derived from biomasses are the best candidates for next generation green NIB due to their abundance, sustainability, environmental benignity and low cost [25]. Although several carbonyl group based organic anodes have been reported for NIB [26-32], the limited cycling stability, low capacity and inferior rate capability impede the application of these carbonyl based organic anodes. The organic anodes face three major challenges: [33-37] (1) The extremely low conductivity of organic materials seriously reduces reaction kinetics, resulting in large overpotentials; (2) Particle pulverization induced by large volume change during sodium ion insertion/extraction accelerates capacity decay; (3) The high solubility of organic materials in organic electrolyte induces active material loss upon cycling, resulting in fast capacity fading. Due to the very low conductivity of organic anodes, 20-30 wt% of conductive carbon has to be added into organic electrodes and the particle size of organic materials has to be reduced into nano-scale to increase the contact surface among organic materials, conductive carbon and electrolytes, thus enhancing electrochemical reaction kinetics [38]. The decrease of organic particle size into nano-scale can also alleviate particle pulverization, further improving cycling stability. Current technology to reduce the solubility of organic compounds in the electrolyte is to increase the polarity of organic compounds by formation of organic salts. Up to date, only nano-size organic salt electrodes show reasonable performance. As battery electrode, the nano-size organic salt electrodes are fabricated through two steps: (1) Synthesizing nano-size organic salts using chemical/physical process; (2) mixing nano-size organic salts with conductive carbon, binder and solvent to form a slurry-ink, and then casting onto current collector.

In this work, 2,5-dihydroxy-1,4-benzoquinone disodium salt (DHBQDS) nanorod anodes were *in situ* fabricated for the first time by one-step process through integrating the nanomaterial synthetic process into electrode casting process, simplifying the electrode preparation process. Due to the high solubility of DHBQDS and sodium alginate binder in water, the DHBQDS-carbon black-sodium alginate aqueous slurry was casted on the Cu foil, and the DHBQDS nanorod crystals and nano-size sodium alginate were uniformly co-precipitated on the carbon surface during the electrode drying process as shown in Figure 1. Due to the fast ionic and electronic conductivity of DHBQDS nanorod-carbon nanocomposite and uniform distribution of DHBQDS, sodium alginate and carbon black, the DHBQDS nanorod electrodes deliver a reversible capacity of 167 mA h g^{-1} at a high current density of 200 mA g^{-1} after 300 cycles, which is 87% of its initial capacity (capacity decay rate of 0.051% per cycle). To reduce the dissolution of DHBQDS in the electrolyte upon cycling, a thin layer of Al_2O_3 with thickness of 1 nm or 2 nm was coated on the DHBQDS nanorod electrodes using ALD. The reversible capacity of Al_2O_3 coated DHBQDS nanorod electrodes remains at 212 mA h g^{-1} at a low current density of 50 mA g^{-1} after 300 cycles with a very low capacity decay rate of 0.049% per cycle. The Al_2O_3 coating remarkably suppresses the dissolution issue as evidenced by the fact that the Coulombic efficiency achieves ~100% for Al_2O_3 coated electrodes after first few cycles. The ALD enhanced organic nanorods represent the best organic anode in Na-ion batteries in terms of reversible capacity and cycle life.

Results and discussion

2,5-Dihydroxy-1,4-benzoquinone disodium salt is synthesized by neutralizing 2,5-dihydroxy-1,4-benzoquinone (DHBQ) with sodium hydroxide in ethanol alcohol solution. DHBQDS contains two carbonyl groups, connected by a benzene ring, and two sodium ions, bonding with phenol groups, as shown in Scheme 1. The 1,4-benzoquinone structure provides two active sites for the redox reaction with electrons and sodium ions, while the sodium-oxygen ionic bonds remarkably decrease its dissolution in organic electrolyte, but maintain high solubility in water. The pristine DHBQDS precipitated from sodium hydroxide-ethanol alcohol solution has a crystal structure as demonstrated by the X-ray diffraction (XRD) pattern in Figure S1a. As shown in Fig. S1b, the pristine DHBQDS particles have irregular rods and particles morphology with an average size about 1 μm. The thermal stability of pristine DHBQDS is measured by thermogravimetric analysis as shown in Figure S1c. Decomposition of DHBQDS molecules starts at the temperature of 150 °C. The DHBQDS lose 4% of weight from 150 °C to 450 °C and 15% of weight from 450 °C to 550 °C during heating in argon.

To investigate the role of carbon black and sodium alginate in precipitation of nano-size DHBQDS, the pristine DHBQDS was recrystallized from four different aqueous solutions/slurries due to the high solubility of DHBQDS in water: (1) DHBQDS-carbon black-sodium alginate aqueous slurry with the weight ratio of 60:25:15; (2) DHBQDS-carbon

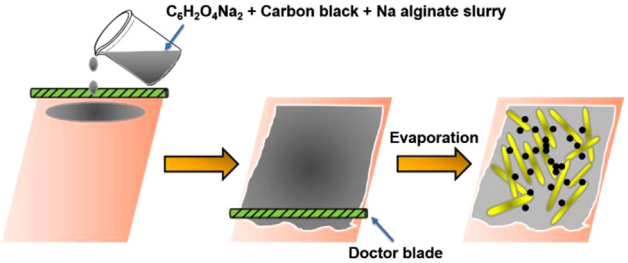

Figure 1 Schematic illustration of nanorod electrode preparation process.

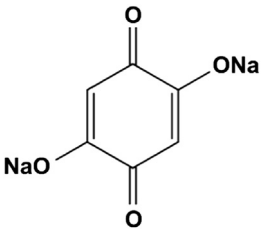

Scheme 1 The molecular structure of DHBQDS.

black aqueous slurry with the same weight ratio (70:30) of DHBQDS to carbon black as in (1); (3) DHBQDS-sodium alginate aqueous solution with the same ratio (80:20) of DHBQDS to sodium alginate as in (1), and (4) aqueous DHBQDS solution. Each slurry/solution was casted on Cu foils and then dried in the vacuum oven at 100 °C for 12 h that is the same procedure as the electrode fabrication process. As shown in Figure 2, DHBQDS precipitated from DHBQDS-carbon black-sodium alginate aqueous solution has nanorod structure with a diameter of 200–300 nm and a length of ~1 μm. However, the DHBQDS precipitated from other three aqueous slurry/solutions have irregular shapes (Figure S2a–c), demonstrating the synergic effect of carbon black and sodium alginate in the formation of DHBQDS nanorods. Therefore, carbon black and sodium alginate binder not only enhance the conductivity and integrity of the electrode, but also assist the growth of DHBQDS nanorods. The exact synergic mechanism of carbon black and sodium alginate for the formation of DHBQDS nanorods is still under investigation. The high solubility of DHBQDS and sodium alginate in water enables the uniform distribution of DHBQDS nanorods, sodium alginate and carbon black in the electrode, which will contribute to the robustness of electrode and superior rate performance of DHBQDS nanorod electrodes.

As shown in Figure 3a, the quinone-based DHBQDS molecule has two carbonyl groups, connected by conjugated structure. Both carbonyl groups can react with sodium ions during sodiation/desodiation process. Therefore, single DHBQDS molecule can reversibly react with two sodium ions and electrons, providing a theoretical capacity of 291 mA h g^{-1}. The cyclic voltammogram (CV) of DHBQDS nanorod electrodes in FEC-based electrolyte in Fig. 3b clearly show two desodiation peaks at 1.39 V and 1.62 V possibly due to the two active carbonyl groups, and two corresponding sodiation peaks can be observed at 1.10 V and 1.16 V after two activation cycles (in the third cycles). The two sodiation peaks are very close to each other, so that they overlap and merge into one broad peak in the following cycles. CV scans demonstrate two pairs of redox peaks, representing two active sites in DHBQDS. The two active carbonyl groups react with sodium ions and electrons step by step to undergo a two-phase transition process.

The electrochemical performance of DHBQDS nanorod electrodes is measured in the coin cells at a current density of 50 mA g^{-1} using sodium metal as a counter electrode. Two electrolytes ($NaClO_4$-EC/DMC and $NaClO_4$-FEC/DMC) are used to investigate the role of FEC on the performance of DHBQDS electrodes. DHBQDS micro-electrode with PVDF binder (Figure S2d) is used as a control to compare with the DHBQDS nanorod electrode. The galvanostatic charge-discharge curves of DHBQDS electrodes at different sodiation/desodiation cycles

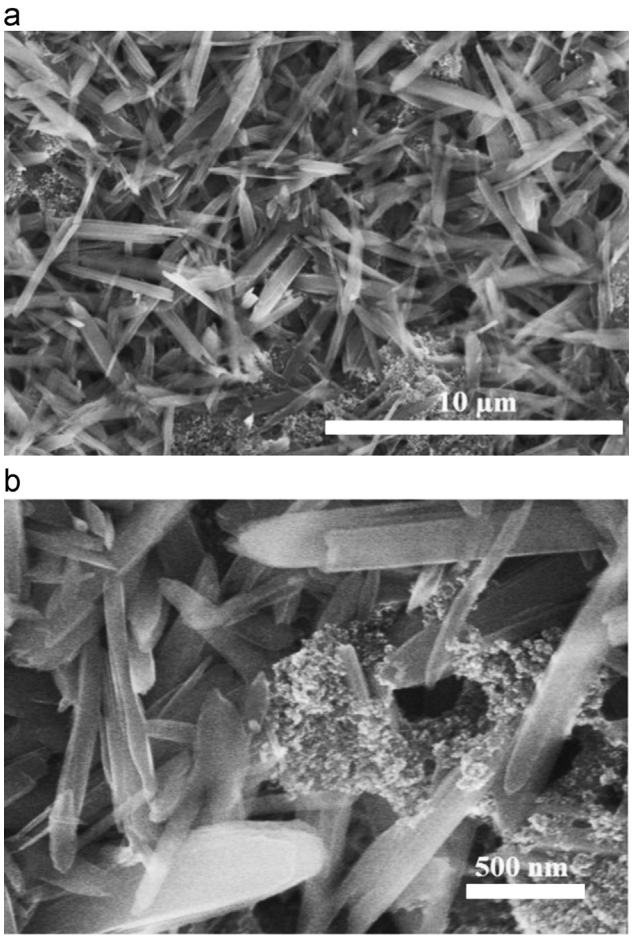

Figure 2 SEM images of DHBQDS nanorod electrode.

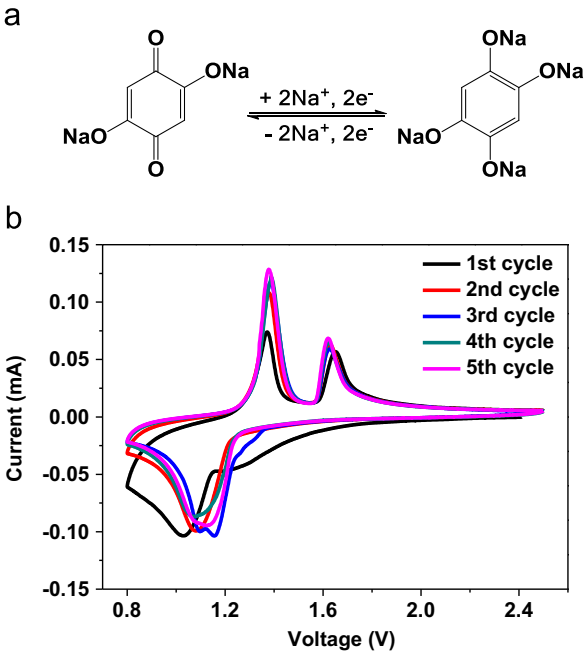

Figure 3 (a) The sodiation/desodiation mechanism for DHBQDS; (b) cyclic voltammogram of DHBQDS electrode with sodium alginate binder in $NaClO_4$-FEC/DMC electrolyte at 0.1 mV s^{-1} in the potential window from 0.5 V to 2.5 V *versus* Na/Na^+.

are shown in Figure 4. One sloping sodiation plateau centered at 1.2 V and two flat desodiation plateaus at 1.3 V and 1.6 V are observed for DHBQDS electrodes in both electrolytes after the first charge/discharge activation cycle, which is consistent with the CV scans in Figure 3. In the first sodiation curve, only one sodiation plateau at 1.2 V is observed in the EC-based electrolyte, while an extra slopping sodiation plateau centered at 1.4 V followed by the regular flat sodiation plateau at 1.2 V can be found in the FEC-based electrolyte, which could be associated to the formation of a thick solid electrolyte interphase (SEI) layer, as evidenced by the larger potential hysteresis between sodiation/desodiation plateaus. Table S1 in supporting information summarizes the capacity and Coulombic efficiency of DHBQDS nanorod electrode and micro-electrode in $NaClO_4$-FEC/DMC and $NaClO_4$-EC/DMC. The first cycle Coulombic efficiencies of DHBQDS nanorod electrode and micro-electrode in $NaClO_4$-FEC/DMC electrolyte are lower than that in EC-based electrolyte, indicating formation of thick SEI layer in FEC-based electrolyte. Moreover, larger overpotential of sodiation/desodiation plateaus can be observed in FEC-based electrolyte owing to the thicker insulating SEI layer. However, SEI layer can reduce the dissolution of DHBQDS and stabilize the electrode, which is beneficial to the long-term cycle life. Table S1 also demonstrates that the reversible capacity of DHBQDS nanorod electrode is higher than that of DHBQDS micro-electrode due to the uniform distribution of DHBQDS nanorods and carbon black after recrystallization.

The cycling stability of DHBQDS electrodes using PVDF and sodium alginate binders was measured in $NaClO_4$-EC/DMC and $NaClO_4$-FEC/DMC electrolytes (Figure 5). As shown in Figure 5a, DHBQDS micro-electrodes using PVDF binder suffers from fast capacity decline in both electrolytes. However, the capacity decay rate of DHBQDS in FEC-based electrolyte is slower than that in EC-based electrolyte, demonstrating that FEC-based electrolyte can improve the cycling stability. Analogous to DHBQDS micro-electrodes with PVDF binder, the cycling performance of DHBQDS nanorod electrodes with sodium alginate binder in the FEC-based electrolyte is also better than that in the EC-based electrolyte (Figure 5b). The reversible capacity of DHBQDS nanorod electrodes in EC-based electrolyte decreases from initial 220 mA h g^{-1} to 92 mA h g^{-1} after 240 cycles, while the reversible capacity of DHBQDS electrodes in FEC electrolyte remains at 190 mA h g^{-1} after 240 cycles corresponding to a low capacity decay rate of 0.13% per cycle. The DHBQDS nanorod electrode using sodium alginate binder show better cycling stability than DHBQDS micro-electrode using

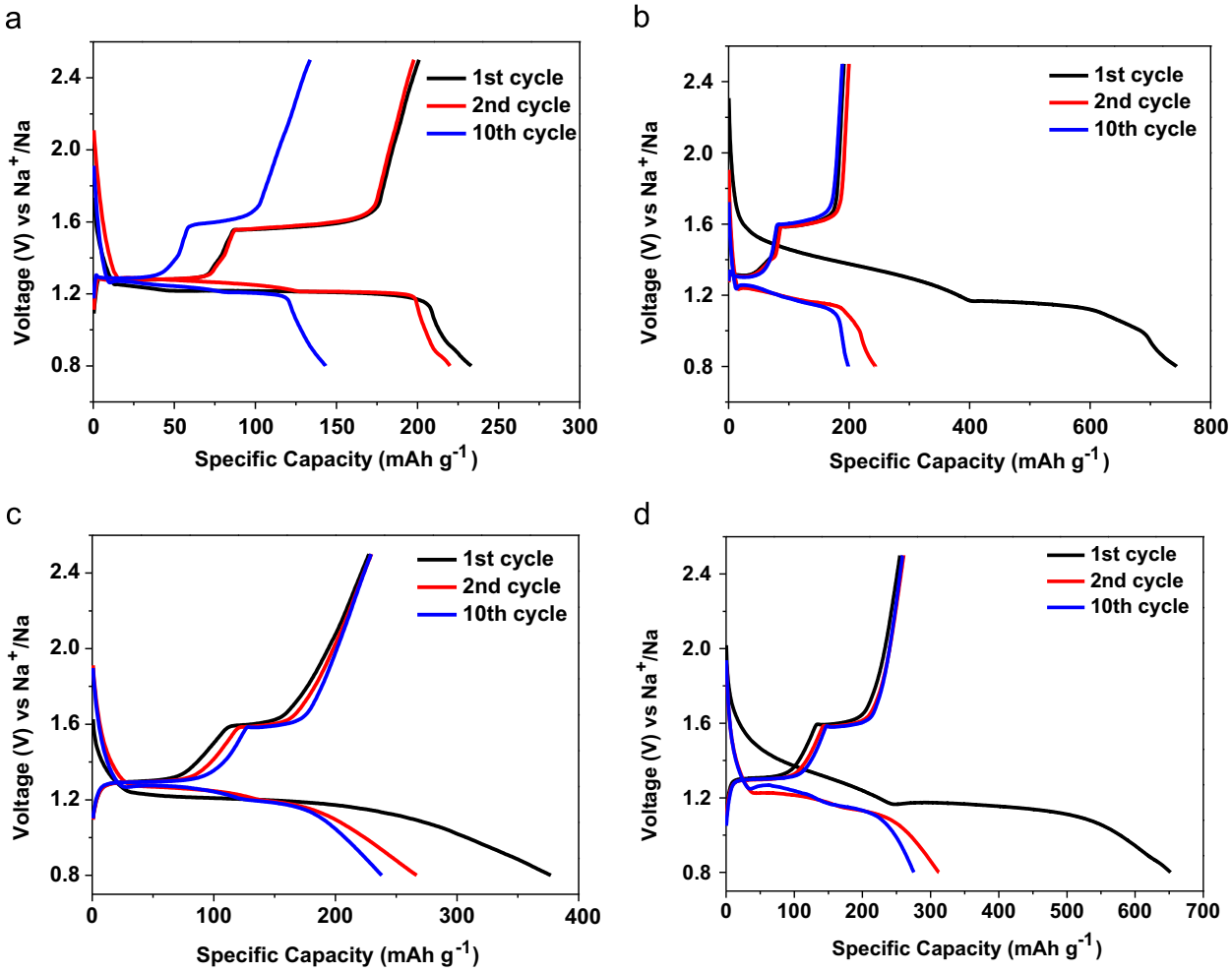

Figure 4 The galvanostatic charge-discharge curves between 0.8 V and 2.5 V *versus* Na/Na^+ for DHBQDS micro-electrode with PVDF binder in $NaClO_4$-EC/DMC electrolyte (a) and $NaClO_4$-FEC/DMC electrolyte (b) and DHBQDS nanorod electrode with sodium alginate binder in $NaClO_4$-EC/DMC electrolyte (c) and $NaClO_4$-FEC/DMC electrolyte (d).

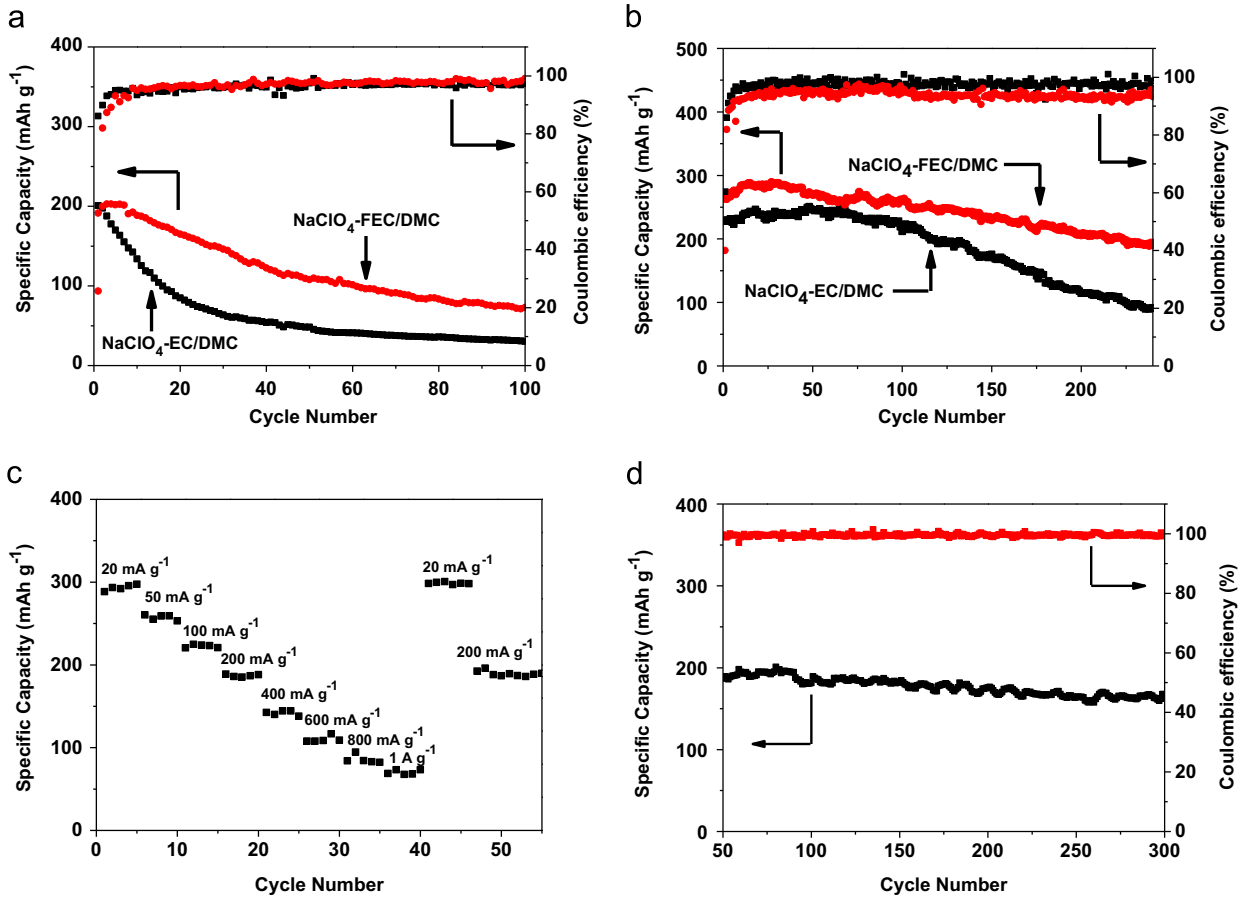

Figure 5 Electrochemical performance of DHBQDS electrode. Desodiation capacity and Coulombic efficiency of DHBQDS micro-electrode with PVDF binder (a) and nanorod electrode with sodium alginate binder (b) in $NaClO_4$-EC/DMC electrolyte and $NaClO_4$-FEC/DMC electrolyte at the current density of 50 mA g^{-1}; (c) rate performance of DHBQDS nanorod electrode with sodium alginate binder in $NaClO_4$-FEC/DMC electrolyte at various current rates; (d) desodiation capacity and Coulombic efficiency after rate measurement at the current density of 200 mA g^{-1}.

PVDF binder in both electrolytes, and DHBQDS nanorod electrodes show the best performance in FEC-based electrolyte. The DHBQDS nanorod formed with the assistance of sodium alginate and carbon black provides larger surface area and shorter ionic/electronic diffusion pathways compared to micro-sized DHBQDS, resulting in fast reaction kinetics. Moreover, the nanostructure can accommodate the volume expansion/shrinkage during sodiation/desodiation process, alleviating the particle pulverization. Since DHBQDS nanorod electrode in FEC-based electrolyte exhibits the best cycle life, it is selected to measure the rate capability. As shown in Figure 5c, with the current density increases from 20 mA g^{-1} to 1 A g^{-1}, the reversible capacity decreases from 290 mA h g^{-1} to 68 mA h g^{-1}, while the reversible capacity recovers to 290 mA h g^{-1} after the current density returns to 20 mA g^{-1}, demonstrating the excellent robustness and integrity of DHBQDS nanorod electrode at various current densities. After 45 cycles, the current density is increased to 200 mA g^{-1} for long term cycling stability test as shown in Figure 5d. By comparing Figure 5b and d, we can conclude that both the cycling stability and Coulombic efficiency of DHBQDS nanorod electrode increase with the elevated current density. The Coulombic efficiency improves from 94% at 50 mA g^{-1} to ~100% at 200 mA g^{-1}, while the reversible capacity remains at 167 mA h g^{-1} at 200 mA g^{-1} after 300 cycles (255 cycles after the rate capability test), which is 87% of its initial capacity (capacity decay rate of 0.051% per cycle). The improved Coulombic efficiency and cycle life at a high charge/discharge current density demonstrate that DHBQDS nanorods still slightly dissolve into the FEC-based electrolyte even SEI protection layer is formed. At low current density, more DHBQDS nanorods can dissolve into the electrolyte, resulting in capacity fading, while the dissolution of DHBQDS nanorods in the electrolyte becomes much slower at high current density due to the shorter charge/discharge period.

The impedance analysis for DHBQDS nano-electrode and micro-electrode in FEC-based electrolyte was performed using electrochemical impedance spectroscopy (EIS). In the impedance plots, the depressed semi-circle in high frequency region represents interface resistance including contact impedance or SEI impedance, and charge transfer impedance, while the low frequency line stands for ion diffusion resistance. As shown in Figure 6, both the interface and diffusion impedances of DHBQDS nano-electrode are much lower than that of DHBQDS micro-electrode, indicating the lower interface resistance and better kinetics of DHBQDS nanorods. The interface resistance of DHBQDS nano-electrode is about 140 Ω, while that for DHBQDS

micro-electrode has much higher value of 280 Ω. The impedance results convince that the high capacity and superior rate capability of DHBQDS nanorod electrode is due to the large electrochemical reaction interface and short lithium ion diffusion pathway.

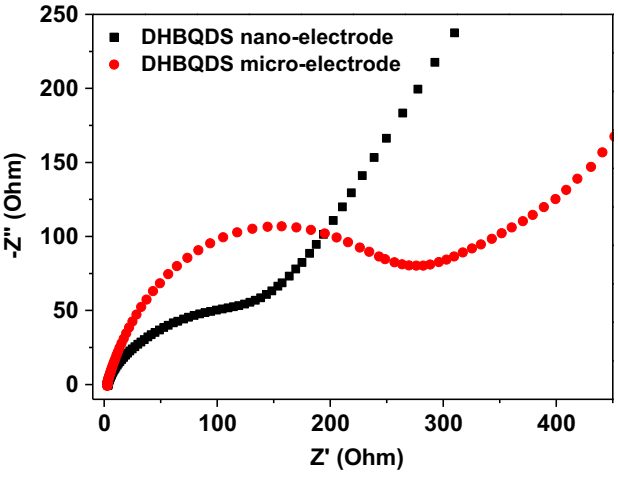

Figure 6 Impedance analysis for DHBQDS nanorod electrode and micro-electrode.

To prevent the DHBQDS nanorods from dissolution into the electrolyte, ALD is employed to deposit a thin layer (1 nm or 2 nm) of Al_2O_3 on the surface of DHBQDS nanorod electrode at 150 °C under vacuum. As shown in Figure S3, negligible morphology change can be observed after uniform Al_2O_3 deposition. The electrochemical performance of Al_2O_3 coated DHBQDS nanorod electrode at a low current density of 50 mA g^{-1} in $NaClO_4$-FEC/DMC electrolyte is shown in Figure 7. The charge/discharge curves of Al_2O_3 covered DHBQDS nanorod electrodes in Fig. 7a and b are similar to that of bare DHBQDS nanorod electrodes in Figure 4d, but the sodiation plateaus shift to negative value and a larger potential hysteresis can be observed, demonstrating the worse reaction kinetics after insulating Al_2O_3 coating. Figure 7c and d shows the cycle life of ALD treated DHBQDS nanorod electrodes. The reversible capacity of both ALD treated electrodes increases in the first twenty cycles due to poor reaction kinetics after insulating Al_2O_3 coating, but the Coulombic efficiency of two electrodes with 1 nm and 2 nm Al_2O_3 increases from 94% of bare DHBQDS to ~100% after nano-layer Al_2O_3 coating, demonstrating the dissolution is alleviated by Al_2O_3 coating. More importantly, the

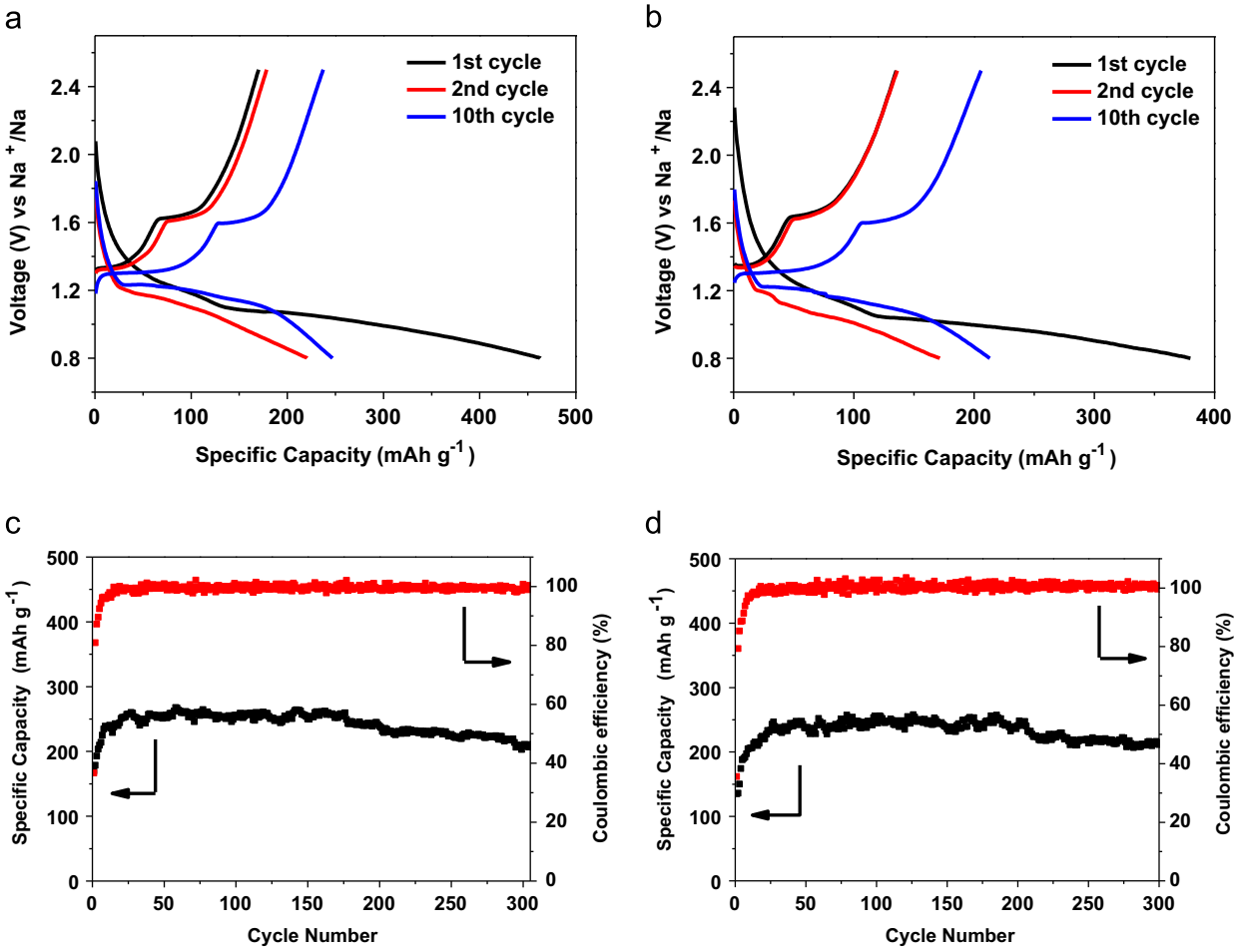

Figure 7 The galvanostatic charge-discharge curves between 0.8 V and 2.5 V *versus* Na/Na^+ for DHBQDS nanorod electrode covered with 1 nm Al_2O_3 layer (a) and 2 nm Al_2O_3 layer (b) with sodium alginate binder in $NaClO_4$-FEC/DMC electrolyte at the current density of 50 mA g^{-1}; desodiation capacity and Coulombic efficiency of DHBQDS nanorod electrode covered with 1 nm Al_2O_3 layer (c) and 2 nm Al_2O_3 layer (d).

reversible capacities of DHBQDS nanorod electrode with 1 nm and 2 nm Al_2O_3 layer remain at 209 mA h g^{-1} and 212 mA h g^{-1} after 300 cycles. The improved Coulombic efficiency and cycle life are attributed to the encapsulation of DHBQDS nanorod by Al_2O_3 layer, which prevents the dissolution of DHBQDS upon cycling. Therefore, a high capacity and long cycle life organic anode is obtained by using organic nanorod material in $NaClO_4$-FEC/DMC electrolyte with Al_2O_3 deposition.

The *ex situ* XRD is performed to study the phase change of DHBQDS nanorod electrode upon sodiation/desodiation process. The fully sodiated DHBQDS nanorod electrode is prepared by sodiating the electrode to 0.8 V and maintaining the voltage at 0.8 V for 12 h. Similarly, the fully desodiated DHBQDS nanorod electrode is prepared by desodiating the electrodes to 2.5 V and maintaining the voltage at 2.5 V for 12 h. Both fully sodiated and fully desodiated electrodes are immersed in dimethyl carbonate for 48 h to remove $NaClO_4$ from the surface of the electrode. From Figure 8, we can observe that the three XRD peaks for fresh DHBQDS at 12.5°, 15.5° and 17° disappear after sodiation, while a small shoulder at 13.3° appears, demonstrating the phase change occurs after sodiation. After desodiation, the small shoulder at 13.3° disappears, and the three XRD peaks for fresh DHBQDS recover, demonstrating DHBQDS nanorods can maintain its crystal structure upon solidation/desolidation cycles. Therefore, the result of *ex situ* XRD confirms that phase change occurs during sodiation/desodiation process, and the crystal structure of DHBQDS nanorod can be maintained after sodiation/desodiation.

Conclusion

A new organic anode material, 2,5-dihydroxy-1,4-benzoquinone disodium salt, was synthesized by neutralizing 2,5-dihydroxy-1,4-benzoquinone with sodium hydroxide in ethanol alcohol solution. For the first time, DHBQDS nanorods were *in situ* synthesized in the electrode fabrication process, which uniquely integrates the nanomaterial synthetic procedure into electrode fabrication process. With the assistance of carbon black and sodium alginate, crystal DHBQDS nanorods were recrystallized from DHBQDS aqueous solution during electrode drying process. The *in situ* formed carbon black–sodium alginate–DHBQDS nanorod composite electrodes have high electronic and ionic conductivity, less particle pulverization, thus high rate capability and excellent cycling stability in $NaClO_4$-FEC/DMC electrolyte. The DHBQDS nanorod electrodes deliver a reversible capacity of 190 mA h g^{-1} at a high current density of 200 mA g^{-1} and maintain 87% of its initial capacity after 300 cycles with capacity decay rate of 0.051% per cycle. ALD is employed to deposit a thin layer (1–2 nm) of Al_2O_3 on the electrode surface, which greatly enhances the Coulombic efficiency from 94% to almost 100% even at a low current density of 50 mA g^{-1}. The reversible capacities of DHBQDS nanorods covered with 1 nm and 2 nm Al_2O_3 layer remain at 209 mA h g^{-1} and 212 mA h g^{-1} after 300 cycles, which represent the best battery performance among all organic anodes. The excellent electrochemical performance of DHBQDS anode demonstrates that it is a promising candidate for advanced NIB. This *in situ* fabrication method can apply to other electrodes if the active materials in electrodes are highly soluble in the solvent of casting slurry.

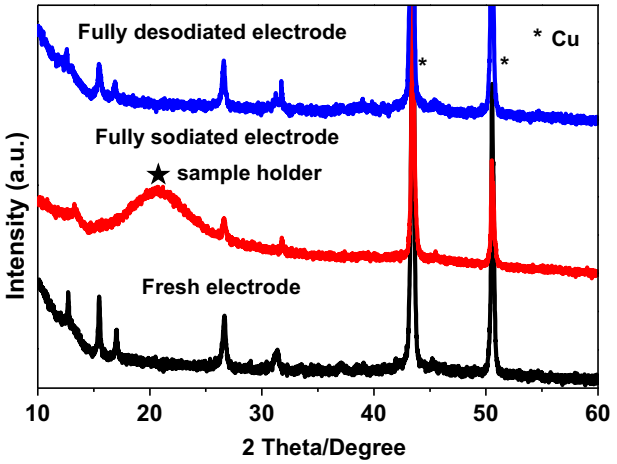

Figure 8 XRD patterns for fresh DHBQDS electrode, fully sodiated DHBQDS electrode and fully desodiated DHBQDS electrode.

Methods

Synthesis of 2,5-dihydroxy-1,4-benzoquinone disodium salt

All chemicals were purchased from Sigma Aldrich and used as received. 2,5-Dihydroxy-1,4-benzoquinone was dispersed in ethanol alcohol with sodium hydroxide powders in 5% excess. The solution was stirred at room temperature for 24 h, and then the solution was filtered to collect the precipitation. The precipitation was washed with ethanol and dried in the vacuum oven at 100 °C overnight. 2,5-Dihydroxy-1,4-benzoquinone disodium salt was collected as orange powder.

Atomic layer deposition

The DHBQDS electrodes were placed into an atomic layer deposition system (Beneq TFS 500) for Al_2O_3 deposition. High-purity nitrogen at 150 °C was used as carrier gas for the whole process. To obtain the Al_2O_3 layer with a thickness of 1 nm or 2 nm, 10 or 20 precursor pulse cycles of ALD-Al_2O_3 were performed. Each cycle included alternating flows of trimethylaluminum (TMA, 4 s, Al precursor) and water (4 s, oxidant) separated by flows of pure nitrogen gas (4 and 10 s, respectively, carrier and cleaning gas). The thickness of Al_2O_3 layer was about 1 Å for each precursor pulse cycle.

Material characterizations

Scanning electron microscopy (SEM) images were taken by Hitachi SU-70 analytical ultra-high resolution SEM (Japan); Thermogravimetric analysis (TGA) was carried out using a thermogravimetric analyzer (TA Instruments, USA) with a heating rate of 5 °C min^{-1} in argon; X-ray diffraction (XRD) pattern was recorded by Bruker Smart1000 (Bruker AXS Inc., USA) using Cu$K\alpha$ radiation. An XRD sample holder with cover is used for the fully sodiated DHBQDS nanorod electrode to avoid its contact with air.

Electrochemical measurements

The DHBQDS powder was mixed with carbon black and sodium alginate/PVDF binder to form a slurry at the weight ratio of 60:25:15. The electrode was prepared by casting the slurry onto copper foil using a doctor blade and dried in a vacuum oven at 100 °C overnight. The slurry coated on copper foil was punched into circular electrodes with an area mass loading of 1.0 mg cm^{-2}. Coin cells for sodium ion batteries were assembled with sodium foil as the counter electrode, 1 M $NaClO_4$ in a mixture of ethylene carbonate/dimethyl carbonate (EC/DMC, 1:1 by volume) or fluoroethylene carbonate/dimethyl carbonate (FEC/DMC, 1:1 by volume) and Celgard® 3501 (Celgard, LLC Corp., USA) as the separator. Electrochemical performance was tested using Arbin battery test station (BT2000, Arbin Instruments, USA). Capacity was calculated on the basis of the mass of DHBQDS. Cyclic voltammograms were recorded using Gamry Reference 3000 Potentiostat/Galvanostat/ZRA with a scan rate of 0.1 mV s^{-1}.

Acknowledgements

This work was supported by the Army Research Lab under Contract no.: W911NF10200. We acknowledge the support of Harry K. Wells Graduate Fellowship and Maryland NanoCenter and its NispLab. The NispLab is supported in part by the NSF as a MRSEC Shared Experimental Facility.

Appendix A. Supporting information

Supplementary data associated with this article can be found in the online version at http://dx.doi.org/10.1016/j.nanoen.2015.03.041.

References

[1] C. Liu, F. Li, L.P. Ma, H.M. Cheng, Adv. Mater. 22 (2010) E28–E62.
[2] M.D. Slater, D. Kim, E. Lee, C.S. Johnson, Adv. Funct. Mater. 23 (2013) 947–958.
[3] V. Palomares, P. Serras, I. Villaluenga, K.B. Hueso, J. Carretero-González, T. Rojo, Energy Environ. Sci. 5 (2012) 5884–5901.
[4] B.L. Ellis, L.F. Nazar, Curr. Opin. Solid State Mater. Sci. 16 (2012) 168–177.
[5] H. Pan, Y. Hu, L. Chen, Energy Environ. Sci. 6 (2013) 2338–2360.
[6] X. Lu, B.W. Kirby, W. Xu, G. Li, J.Y. Kim, J.P. Lemmon, V.L. Sprenkle, Z. Yang, Energy Environ. Sci. 6 (2013) 299–306.
[7] S. Xin, Y.X. Yin, Y.G. Guo, L.J. Wan, Adv. Mater. 26 (2014) 1261–1265.
[8] C. Luo, Y. Xu, Y. Zhu, Y. Liu, S. Zheng, Y. Liu, A. Langrock, C. Wang, ACS Nano 7 (2013) 8003–8010.
[9] A. Abouimrane, D. Dambournet, K.W. Chapman, P.J. Chupas, W. Weng, K. Amine, J. Am. Chem. Soc. 134 (2012) 4505–4508.
[10] M. Yabuuchi, M. Kajiyama, J. Iwatate, H. Nishikawa, S. Hitomi, R. Okuyama, R. Usui, Y. Yamada, S. Komaba, Nat. Mater. 11 (2012) 512–517.
[11] M. Guignard, C. Didier, J. Darriet, P. Bordet, E. Elkaïm, C. Delmas, Nat. Mater. 12 (2013) 74–80.
[12] J. Billaud, G. Singh, A.R. Armstrong, E. Gonzalo, V. Roddatis, M. Armand, T. Rojo, P.G. Bruce, Energy Environ. Sci. 7 (2014) 1387–1391.
[13] Y. Zhu, Y. Xu, Y. Liu, C. Luo, C. Wang, Nanoscale 5 (2013) 780–787.
[14] A. Langrock, Y. Xu, Y. Liu, S. Ehrman, A. Manivannan, C. Wang, J. Power Sources 223 (2013) 62–67.
[15] P. Barpanda, G. Oyama, S. Nishimura, S.C. Chung, A. Yamada, Nat. Commun. 5 (2014) 4358.
[16] S. Komaba, W. Murata, T. Ishikawa, N. Yabuuchi, T. Ozeki, T. Nakayama, A. Ogata, K. Gotoh, K. Fujiwara, Adv. Funct. Mater. 21 (2011) 3859–3867.
[17] E.M. Lotfabad, J. Ding, K. Cui, A. Kohandehghan, W.P. Kalisvaart, M. Hazelton, D. Mitlin, ACS Nano 8 (2014) 7115–7129.
[18] Y. Xu, Y. Zhu, Y. Liu, C. Wang, Adv. Energy Mater. 3 (2013) 128–133.
[19] H. Zhu, Z. Jia, Y. Chen, N. Weadock, J. Wan, O. Vaaland, X. Han, T. Li, L. Hu, Nano Lett. 13 (2013) 3093–3100.
[20] A. Darwiche, C. Marino, M.T. Sougrati, B. Fraisse, L. Stievano, L. Monconduit, J. Am. Chem. Soc. 134 (2012) 20805–20811.
[21] J. Qian, X. Wu, Y. Cao, X. Ai, H. Yang, Angew. Chem. Int. Ed. 52 (2013) 4633–4636.
[22] Y. Kim, Y. Park, A. Choi, N.S. Choi, J. Kim, J. Lee, J.H. Ryu, S.M. Oh, K.T. Lee, Adv. Mater. 25 (2013) 3045–3049.
[23] J. Wang, C. Luo, T. Gao, A. Langrock, A.C. Mignerey, C. Wang, Small 11 (2015) 473–481.
[24] Z. Hu, L. Wang, K. Zhang, J. Wang, F. Cheng, Z. Tao, J. Chen, Angew. Chem. Int. Ed. 53 (2014) 12794–12798.
[25] Y. Liang, Z. Tao, J. Chen, Adv. Energy Mater. 2 (2012) 742–769.
[26] Y. Park, D.S. Shin, S.H. Woo, N.S. Choi, K.H. Shin, S.M. Oh, K.T. Lee, S.Y. Hong, Adv. Mater. 24 (2012) 3562–3567.
[27] A. Abouimrane, W. Weng, H. Eltayeb, Y. Cui, J. Niklas, O. Poluektov, K. Amine, Energy Environ. Sci. 5 (2012) 9632–9638.
[28] L. Zhao, J. Zhao, Y.-S. Hu, H. Li, Z. Zhou, M. Armand, L. Chen, Adv. Energy Mater. 2 (2012) 962–965.
[29] S. Wang, L. Wang, Z. Zhu, Z. Hu, Q. Zhao, J. Chen, Angew. Chem. Int. Ed. 53 (2014) 5892–5896.
[30] C. Luo, Y. Zhu, Y. Xu, Y. Liu, T. Gao, J. Wang, C. Wang, J. Power Sources 250 (2014) 372–378.
[31] J. Xiang, C. Chang, M. Li, S. Wu, L. Yuan, J. Sun, Cryst. Growth Des. 8 (2008) 280–282.
[32] K. Liu, J. Zheng, G. Zhong, Y. Yang, J. Mater. Chem. 21 (2011) 4125–4131.
[33] H. Kim, D.-H. Seo, G. Yoon, W.A. Goddard, Y.S. Lee, W.-S. Yoon, K. Kang, J. Phys. Chem. Lett. 5 (2014) 3086–3092.
[34] C. Luo, R. Huang, R. Kevorkyants, M. Pavanello, H. He, C. Wang, Nano Lett. 14 (2014) 1596–1602.
[35] Z. Song, Y. Qian, X. Liu, T. Zhang, Y. Zhu, H. Yu, M. Otani, H. Zhou, Energy Environ. Sci. 7 (2014) 4077–4086.
[36] H. Chen, M. Armand, G. Demailly, F. Dolhem, P. Poizot, J.M. Tarascon, ChemSusChem 1 (2008) 348–355.
[37] M. Armand, S. Grugeon, H. Vezin, S. Laruelle, P. Ribière, P. Poizot, J.M. Tarascon, Nat. Mater. 8 (2009) 120–125.
[38] S. Wang, L. Wang, K. Zhang, Z. Zhu, Z. Tao, J. Chen, Nano Lett. 13 (2013) 4404–4409.

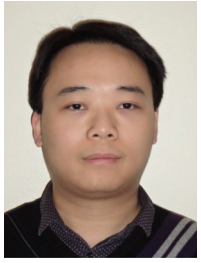

Mr. Chao Luo is currently a Ph.D. candidate with Professor Chunsheng Wang in Department of Chemical and Biomolecular Engineering, University of Maryland, College Park. He received his Bachelor's Degree in College of Chemistry and Molecular Sciences from Wuhan University in 2008. Afterwards, he got his Master's Degree with Professor Xuesong Wang in Technical Institute of Physics and Chemistry, Chinese Academy of Sciences in 2011. He is mainly interested in organic electrode materials and carbon coated sulfur/selenium composites for energy application.

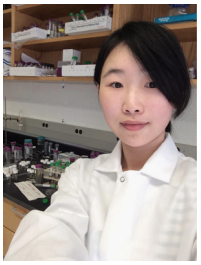

Ms. Jingjing Wang received her Bachelor's Degree from Wuhan University in 2008 and her Master's Degree from Chinese Academy of Sciences in 2011. She is a currently a joint Ph.D. student as co-advised by Prof. Alice Mignerey in Chemistry department and Prof. Chunsheng Wang in Chemical Engineering. Her research interests include layered metal sulfides for high performance lithium and sodium storage, charge and discharge mechanism study and the reasoning for battery malfunction during extended cycling.

Dr. Xiulin Fan received his Ph.D. in Materials Science and Engineering from Zhejiang University in 2012. He is currently a postdoctor at University of Maryland-College Park. His research interests are novel nanostructured materials and their application in energy storage and conversion devices including lithium-ion batteries, sodium-ion batteries and hydrogen storage.

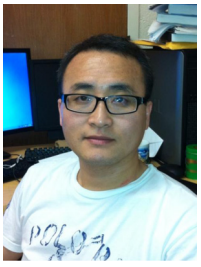

Dr. Yujie Zhu received his B.S. Degree in Chemical Engineering from Tsinghua University, and earned his Ph.D. Degree in Chemical and Biomolecular Engineering in 2013 from University of Maryland, College Park (UMCP). He is now a postdoctoral research associate in Professor Chunsheng Wang's research group at UMCP. His research focuses on development of electrochemical techniques for phase transition electrode materials, investigation of charge/discharge process for single particle systems by *in-situ* transmission electron microscopy, and electrode materials synthesis for lithium-/sodium-ion batteries.

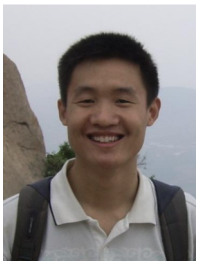

Mr. Fudong Han received his B.S. and M.S. Degree in Materials Science and Engineering from Shandong University, and is currently a Ph.D. student at Department of Chemical and Biomolecular Engineering at University of Maryland, College Park. His research focuses on all-solid-state lithium-ion batteries with the aim to minimize the interfacial resistance between the electrodes and electrolyte.

Dr. Liumin Suo received his Ph.D. in condensed matter physics in 2013 at Institute of Physics, Chinese Academy of Sciences. He is currently postdoctoral Research Associate in University of Maryland, College Park, USA. His research interests focus on energy storage devices including electrode materials, electrolyte and electrochemistry for rechargeable batteries (rechargeable lithium ion and lithium metal batteries).

Prof. Chunsheng Wang is an associate professor at University of Maryland College Park (UMCP). He was educated in materials science and trained in electrochemistry. He has more than 120 peer-reviewed journal publications and more than 20 years of experience in battery research. His research work has been cited more than 4500 times with h index of 38. His Li-ion battery research has been highlighted in EFRC news by DoE in 2012, and by Chemical & Engineering News in 2013. He is a recipient of the University of Maryland Outstanding junior Researcher Award.